Journal of
Low Power Electronics and Applications

MDPI

Article

Optimized Coupling Coil Geometry for High Wireless Power Transfer Efficiency in Mobile Devices

Fahad M. Alotaibi

Department of Information Systems, Faculty of Computing and Information Technology (FCIT), King Abdulaziz University Jeddah, Jeddah 34025, Saudi Arabia; fmmalotaibi@kau.edu.sa

Abstract: Wireless Power Transfer (WPT) enables efficient, contactless charging for mobile devices by eliminating mechanical connectors and wiring, thereby enhancing user experience and device longevity. However, conventional WPT systems remain prone to performance issues such as coil misalignment, resonance instability, and thermal losses. Addressing these challenges involves designing coil geometries that operate at lower resonant frequencies to strengthen magnetic coupling and decrease resistance. This work introduces a WPT system with a performance-driven coil design aimed at maximizing magnetic coupling and mutual inductance between the transmitting (Tx) and receiving (Rx) coils in mobile devices. Due to the nonlinear behavior of magnetic flux and the high computational cost of simulations, exploring the full design space for coils using ANSYS Maxwell becomes impractical. To address this complexity, a machine learning (ML)-based optimization framework is developed to efficiently navigate the design space. The framework integrates a hybrid sequential neural network and multivariate regression model to optimize coil winding and ferrite core geometry. The optimized structure achieves a mutual inductance of 12.52 μH with a conventional core, outperforming many existing ML models. Finite element simulations and experimental results validate the robustness of the method, which offers a scalable solution for efficient wireless charging in compact, misalignment-prone environments.

Keywords: wireless power transfer; optimization; coil structuring; hybrid neural networks; machine learning

check for updates

Academic Editor: Xiaoxi Liu

Received: 15 April 2025
Revised: 28 May 2025
Accepted: 5 June 2025
Published: 17 June 2025

Citation: Alotaibi, F.M. Optimized Coupling Coil Geometry for High Wireless Power Transfer Efficiency in Mobile Devices. *J. Low Power Electron. Appl.* **2025**, *15*, 36. https://doi.org/10.3390/jlpea15020036

Copyright: © 2025 by the author. Licensee MDPI, Basel, Switzerland. This article is an open access article distributed under the terms and conditions of the Creative Commons Attribution (CC BY) license (https://creativecommons.org/licenses/by/4.0/).

1. Introduction

Unlocking the future of power delivery, wireless charging systems based on inductive power transfer (IPT)—widely known as wireless power transfer (WPT)—are rapidly emerging as efficient and contactless energy solutions. WPT enables the transfer of electrical energy from an external power source to a remote receiving device without requiring any physical connection or conduction medium. Extensive research has been conducted on various aspects of WPT systems, including coil design [1], core design [2], compensation topology [3], rotational invariance coil [4], and power conversion control [5]. Among them, the design of IPT coils is crucial for optimizing both power efficiency and performance in WPT systems. Building on recent developments, this paper presents a coil design tailored to maximize coupling efficiency in wireless power transfer (WPT) systems for mobile applications. The inherent nonlinearity of the electromagnetic field complicates the use of traditional analytical approaches, making it challenging to achieve optimal design performance through conventional methods. To address this, a machine learning framework is proposed to optimize the WPT system.

Significant attention has been focused on iterative approaches to optimize the structural geometry of IPT coils, particularly in achieving optimal design parameters. However, less emphasis has been placed on optimizing the geometry using machine learning techniques, which serve as an efficient approach for learning nonlinear data. The optimal coil design minimizes volume, weight, and cost while significantly improving the power transfer efficiency of the WPT system. Conventionally, the design of coil layouts within WPT systems has relied on intuition and iterative simulation-based analysis [6]. However, analytical modeling using electromagnetic principles remains challenging because of the complex and non-uniform magnetic behavior introduced by copper windings. As a result, prior research has largely relied on computational simulations or data-driven approaches to investigate how variations in coil geometry influence the resulting magnetic field patterns. Recognizing the limitations of conventional methods, we propose a novel machine learning-based approach for designing the geometry of copper windings in IPT systems. Using machine learning techniques to analyze the nonlinear behavior of the magnetic field in WPT, our approach aims to learn the characteristics of magnetic field distortion caused by ferrite cores and to determine optimal coil geometry and ferrite core layouts to achieve high coupling between the WPT coils. Our machine learning algorithm utilizes simulation-based data obtained through Ansys Maxwell, using the Finite Element Analysis (FEA) method. The limited data obtained with Ansys is used for training the proposed machine learning framework. This framework aims to estimate the geometry of the copper coil and ferrite core, which offers a high coupling coefficient between the Tx and Rx coils in wireless charging systems of mobile devices. The proposed framework not only optimizes the WPT coil structure to enhance mutual coupling but also reduces the weight and cost of the overall WPT system.

The primary contributions to optimizing the coil geometry of the WPT system are outlined below:

- This work introduces ResML-HybNN, an innovative hybrid neural architecture that combines GRU, LSTM, and BiLSTM units within a residual multi-layer framework. The model incorporates ReLU activation, normalization, and dropout techniques to improve training stability, generalization, and optimization efficiency. The architecture incorporates skip connections, enabling direct feature propagation across parallel and cascaded blocks, mitigating vanishing gradients, and strengthening feature representation in deep network layers.
- An iterative approach is utilized to improve the generation of training data through Ansys simulations. Additionally, the architecture of the ResML-HybNN model is refined through iterative simulations, where key hyperparameters—such as hidden unit count, dropout probability, learning rate, and number of training epochs—are systematically optimized using parametric analysis.
- A stratified clustering approach is employed to obtain a uniformly distributed sample from the design space, providing an effective starting point for model training and mitigating training bias. The optimized designs are further validated through experimental measurements following fabrication.

The remaining sections of this paper are organized as follows: Section 2 presents the related work and foundational concepts in detail. Section 3 describes the proposed methodology, including the framework and the architecture of the neural network. Sections 4 and 5 provides a detailed analysis of the experimental results, supported by plots and oscilloscope graphs. Finally, Section 6 concludes the paper.

2. Related Work

Wireless power transfer (WPT) systems have gained significant interest from researchers, particularly in the areas of miniaturization and improved coupling of WPT devices [7]. Recent advancements have enabled the application of modern machine learning techniques to optimize the structural geometry and key parameters of WPT systems [8]. Various machine learning frameworks, such as handcrafted feature extraction methods and Convolutional Neural Networks (CNNs), have been employed by researchers under the specific requirements of their applications [9]. While handcrafted features created through feature engineering are adept at capturing specific aspects of the data, they often overlook other relevant factors. In contrast, the performance of deep neural networks is predominantly determined by the quality and diversity of the training dataset [10]. Handcrafted techniques previously employed for 2D visual data representation tasks often struggle with challenges such as variations in illumination, scale, orientation, clutter, blurriness, and other sources of noise [11]. These handcrafted descriptors typically focus on extracting texture and contour features from the 2D input data but tend to overlook the broader shape information of the objects themselves [11]. To enhance the rotation invariance and discriminative power of descriptors, the Rotation Invariant Uniform (RIU) was introduced in the Local Binary Pattern framework [12]. However, these handcrafted methods typically rely on isolated classification approaches, such as Support Vector Machines (SVM), K-Nearest Neighbors (KNN), and Decision Tree classifiers, to classify the extracted features in supervised settings. To improve robustness and invariance, researchers often adopt ensemble methods that combine multiple feature descriptors into more robust feature vectors [13]. In contrast, WPT systems, which involve coil and core geometries, present a wide range of possible patterns with minimal interclass variation. While handcrafted feature extraction models struggle to scale to large datasets, deep learning approaches offer a solution by effectively handling the vast and complex patterns found in WPT systems, overcoming the scalability limitations of traditional methods [14].

In recent years, the fields of data science and machine learning have gained considerable attention for optimization tasks, with techniques such as artificial neural networks (ANN), swarm intelligence (SI), and evolutionary computation (EC) methods - including genetic algorithms (GA) and particle swarm optimization (PSO) - playing pivotal roles [15]. Both PSO and GA are iterative methods that evolve over multiple generations to converge on optimal solutions. However, a key difference between them lies in their mechanisms: PSO does not utilize evolutionary operators such as crossover or mutation. Instead, it relies on the movement of particles through the search space, where each particle is guided by the best-performing ones. In contrast, ANNs adjust the weights between neurons during the learning process, making them particularly adept at addressing complex, nonlinear problems. This capability allows ANNs to excel in applications like adaptive control and function approximation, where they can handle imprecise data and establish nonlinear mappings [16]. Specifically, in the realm of WPT, ANN-based optimization techniques are typically focused on enhancing power transfer efficiency (PTE). To evaluate the performance of the ANN model, its results are often compared with those obtained from FEM simulations, with ANSYS Maxwell (Version 2023 R2, Always Ansys, Inc., San Diego, CA, USA) being a commonly used tool for such analysis.

Convolutional neural networks (CNNs) and deep neural networks (DNNs) are widely used in machine learning-driven optimization tasks [14]. To tackle multi-objective optimization in WPT systems—specifically minimizing core volume and magnetic losses—a genetic algorithm is employed, with an artificial neural network (ANN) serving as the fitness function. This approach replaces traditional FEA methods, significantly accelerating the optimization process [17]. Although using an ANN as a surrogate model speeds up

the optimization, the accuracy of the results is heavily reliant on the quality of the ANN's training. In contrast, ref. [18] explores an innovative approach in which genetic algorithms (GA) are applied to optimize the weights of a neural network, thus enhancing the performance of the optimized weights. Another notable advancement is presented in [19], where a Reinforcement Learning (RL) algorithm is utilized to optimize the geometry of the ferromagnetic core, c core, improving the coupling of the Tx and the Rx coil of a WPT system at a distance of 98 cm. Additionally, ref. [19] combines RL with ϵ-greedy Q-learning, achieving a 2% increase in mutual inductance and a 50% reduction in computational time. While RL provides substantial reductions in computational cost, it is often prone to converging to local optima instead of finding the global optimum. Due to the limited size of the simulation dataset, transformer-based and CNN-LSTM models were not adopted in this study, but they will be explored in future work as the dataset is expanded.

In the realm of WPT, a comprehensive review of various machine learning techniques, including supervised and unsupervised learning, is provided in [20]. This review explores a range of architectures, including convolutional neural networks (CNNs), deep belief networks, autoencoders, recurrent models (RNNs), deep reinforcement learning frameworks, and generative adversarial networks (GANs), highlighting their individual advantages and limitations. CNNs are typically hindered by issues related to low accuracy and high computational demands [21], while auto-encoder networks struggle with large datasets [22]. Deep Belief Networks (DBNs) often demand high-performance hardware resources for efficient training [23], while Recurrent Neural Networks (RNNs) tend to exhibit increased computational complexity when processing large-scale datasets [24]. Reinforcement Learning is limited in its ability to detect communication attacks [25], and GANs are often criticized for their computational complexity [26]. Considering the strengths and limitations of these AI algorithms, we propose a hybrid and residual supervised network architecture that integrates Gated Recurrent Units (GRUs) and Long Short-Term Memory (LSTM) networks in a combined residual and hybrid configuration. The proposed framework and its performance results are detailed in the following sections.

3. Methodology

The machine learning-based structuring of the WPT coil is presented in a detailed outline of the neural network. The proposed optimization strategy focuses on determining the geometric parameters of the planar spiral TX and RX coils using the ResML-HybNN sequential hybrid network while the conventional solid ferrite core structure is considered. Optimization of TX and RX coils involves identifying key geometric parameters, including wire thickness, inner radius, radius variation, and number of turns, to achieve the highest mutual inductance. The optimization process evaluates multiple configurations of the ResML-HybNN deep neural network (DNN) to determine the optimal design that maximizes mutual inductance while ensuring that flux and temperature remain within FDA-defined limits.

3.1. Design Setup and Constraints

The geometric parameters of the WPT RX coil are designed to fit within the compact dimensions of the casing of the mobile device, with its components optimized for this limited space. The titanium casing, shown in Figure 1, houses the RX coil within a 40 mm × 40 mm × 1.1 mm space. Due to the limited space, the RX coil adopts a planar configuration. The coil wire and the feed line, with uniform thicknesses ranging from 0.1 to 0.55 mm, are commercially available and compatible with copper wires, as used in the machine learning framework. Varying wire thicknesses, turn counts, inner radii, and turn spacings allow the design of approximately 0.35 million valid coil structures to fit within

the casing. Simulating all these designs in Ansys Maxwell would take years, so a machine learning framework is employed to optimize the coil parameters. The RX coil is placed approximately 3 mm below the casing, with a 3 mm gap between its upper edge and the casing. The path between the TX and RX coils is obstructed by 1 mm of titanium and 2 mm of air inside the casing.

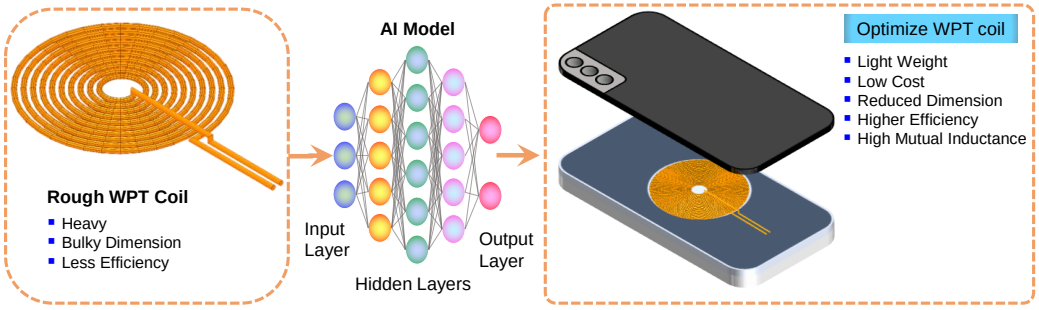


Figure 1. Generalized framework illustrating the optimization of a raw IPT coil, along with casing details of the optimized coil within mobile devices.

3.2. Deep Learning Model for Wireless Power Transfer Efficiency Prediction

The proposed WPT optimization framework, illustrated in Figure 2, employs an iterative learning approach to enhance the precision of the ResML-HybNN model by leveraging high-quality training samples for the estimation of the rewards in all input cases. Initially, training data are generated through stratified clustering, partitioning the input space into $k = 300$ clusters. The centroids of these clusters serve as training input, with their reward values determined through FEA simulations in Ansys-Maxwell. This clustering method ensures data uniformity and reduces bias in model training. The trained model predicts reward values for all test cases in each iteration, identifying configurations with high mutual inductance. These high-performance cases are validated using Ansys simulations, and the top 20 results from each iteration are incorporated into the training set. This iterative refinement progressively improves the dataset, ultimately estimating the optimal coil structure. The proposed ResML-HybNN model is trained on a dataset in which power transfer efficiency (PTE) serves as the reward metric for all input coil parameters. It predicts reward values for test samples, facilitating the identification of the optimal coil structure. As depicted in Figure 3, the model architecture comprises three sequential blocks of deep neural networks (DNN), followed by a K-Nearest Neighbors (KNN) regressor. Each DNN block integrates six essential layers: a sequential neural network, batch normalization, dropout, ReLU activation, a fully connected layer, and a regression layer. The three deep neural network (DNN) modules incorporate Gated Recurrent Units (GRU), Long Short-Term Memory (LSTM), and Bidirectional LSTM (BiLSTM) architectures, respectively, to facilitate robust temporal feature extraction and optimization.

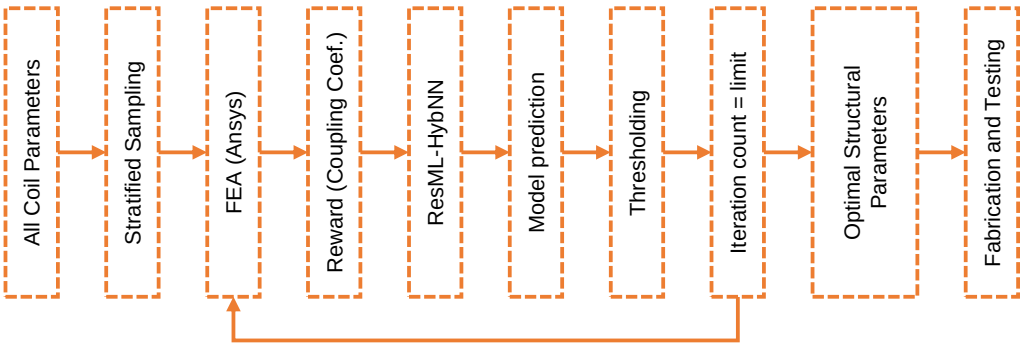


Figure 2. Framework of the proposed multi-objective optimization algorithm.

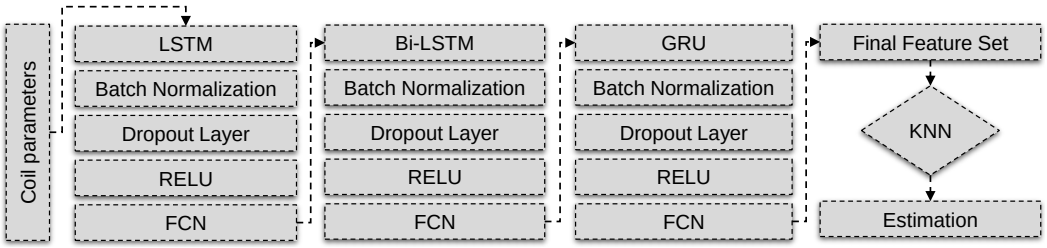


Figure 3. Proposed hybrid and residual layer-based sequential neural network (ResML-HybNN).

Let the input vector $\mathbf{z} \in \mathbb{R}^N$ denote the set of geometric parameters N that characterize the coil design at each time step. These input vectors form a temporal sequence $\{\mathbf{z}_1, \mathbf{z}_2, \ldots, \mathbf{z}_T\}$, where T is the total number of time steps. This sequence is processed by a long-short-term memory (LSTM) network that is adept at learning long-term dependencies within sequential data. Using gating mechanisms, the LSTM maintains an internal memory cell to regulate the flow of information throughout the time steps. The following compact operation can summarize its behavior at each step t:

$$(\mathbf{h}_t, \mathbf{c}_t) = \text{LSTM}(\mathbf{z}_t, \mathbf{h}_{t-1}, \mathbf{c}_{t-1})$$

Here, $\mathbf{h}_t \in \mathbb{R}^d$ represents the hidden state (or output) at time step t, $\mathbf{c}_t \in \mathbb{R}^d$ is the state of memory cells, and d is the dimensionality of the hidden representation. The LSTM utilizes previous hidden and cell states $\mathbf{h}_{t-1}$ and $\mathbf{c}_{t-1}$, along with the current input $\mathbf{z}_t$, to compute the updated states.

To capture both past and future contextual dependencies, the output from the LSTM is passed through a Bidirectional LSTM (BiLSTM) layer. Unlike standard LSTM, the BiLSTM processes the input sequence in two directions: forward (from $t = 1$ to T) and backward (from $t = T$ to 1). Let $\mathbf{h}_t^f$ and $\mathbf{h}_t^b$ denote the hidden states from the forward and backward passes, respectively. The BiLSTM output at time step t is obtained by concatenating these two directional states:

$$\mathbf{h}_t^{\text{bi}} = \left[\mathbf{h}_t^f \parallel \mathbf{h}_t^b\right]$$

where $\parallel$ indicates the concatenation of vectors. This combined representation provides a more comprehensive encoding of the temporal structure by incorporating information from the preceding and subsequent time steps.

Subsequently, the output $\mathbf{h}_t^{\text{bi}}$ is fed into a Gated Recurrent Unit (GRU) layer. GRUs are a simplified variant of LSTMs that merge the forget and input gates into a single update gate, reducing computational complexity while retaining memory capabilities. The GRU updates its hidden state based on the BiLSTM output and its previous hidden state:

$$\mathbf{h}_t^g = \text{GRU}(\mathbf{h}_t^{\text{bi}}, \mathbf{h}_{t-1}^g)$$

where $\mathbf{h}_t^g \in \mathbb{R}^d$ is the hidden state of the GRU at time t. This stage refines the temporal features extracted from the sequence.

Finally, the last hidden state $\mathbf{h}_T^g$, or a suitable aggregation over time, is used as a fixed-length feature vector that summarizes the entire sequence. This vector is input to a K-Nearest Neighbors (KNN) classifier. KNN operates by calculating the distances between the test vector and the training vectors stored in the feature space. A class label is assigned to the test sample based on the majority class among the k closest vectors (nearest neighbors):

$$\hat{y} = \text{KNN}(\mathbf{h}_T^g, \mathcal{D})$$

where $\hat{y}$ is the predicted label and $\mathcal{D}$ denotes the training dataset in the GRU feature space. This combination of deep sequential modeling (LSTM, BiLSTM, GRU) with a classical,

non-parametric classifier (KNN) enables the model to effectively learn complex patterns in the coil design data and generalize well to new instances.

4. Results and Discussion

4.1. Simulation Results

HRL-SeqNet performance for coil has been analyzed and compared with recently reported regression networks. Parametric optimization was conducted through extensive experimentation. The final optimal networks were utilized for estimating coil structures, while the SVR and the DQN networks were utilized for core optimizations to enhance the Mutual inductance and reduce ferrite.

4.2. ResML-HybNN Optimization Performance

The proposed ResML-HybNN framework comprises three distinct regression neural network blocks arranged in sequence, followed by a regression layer of k-nearest neighbors (kNN). The architectural layout and internal parameter configurations of each neural block are thoroughly investigated. In the ResML-HybNN framework, each neural network block consists of a sequential neural layer followed by batch normalization, a dropout layer (with a rate of 0.1), a ReLU activation function, and a fully connected network (FCN), collectively forming a regression block. The inclusion of 8 hidden units and dropout helps mitigate overfitting and prevents issues such as vanishing or exploding gradients. Each block in the ResML-HybNN architecture serves as a feature descriptor, contributing to the overall representation of the input. Within each block, the ReLU layer plays a role in managing nonlinearity both in the extracted features and during the feature aggregation process based on fully connected networks (FCNs). The features derived from the trained blocks are subsequently combined to form the test feature vector, which is then used in k-nearest neighbors (kNN) regression. To ensure the extracted features are both distinctive and robust, the neural layer parameters and configurations are meticulously optimized.

Among the 0.3 million possible coil geometries, only 300 uniformly distributed samples—amounting to just 0.001% of the total design space—are used to train the ResML-HybNN model. These training samples are selected using stratified clustering to ensure representative coverage. Stratified clustering ensures that the selected samples are diverse and representative, improving the model's ability to generalize across the entire design space despite the small sample size. The performance of the proposed ResML-HybNN is evaluated on test data using the mean square error (MSE) metric. The Mean Squared Error (MSE) is calculated by comparing the power transfer efficiency estimated by the proposed ResML-HybNN model with that obtained from Ansys Maxwell, using the same set of input test samples. This evaluation serves to validate the network's architecture, configuration, and parameter tuning. The ResML-HybNN's MSE is also benchmarked against other regression models, and it achieves the lowest MSE, indicating that its predicted reward values closely align with those from Ansys. For this analysis, 100 randomly selected test cases were used. A performance comparison between ResML-HybNN and recent related works is presented in Table 1.

As presented in Table 1, the proposed ResML-HybNN achieves a mean squared error (MSE) of 6.371×10^{-10} for coupling coefficient estimation, outperforming the second-best model by a factor of 1.04. It also achieves the lowest MSE of 1.51×10^{-8} for mutual inductance prediction. Although the HRL-SeqNet achieves the best overall accuracy across both coupling coefficient and mutual inductance estimations, linear regression yields slightly better results for magnetic flux prediction. Since the focus of this study is on mutual inductance and coupling coefficient, the ResML-HybNN is selected for coil geometry estimation. The model performance is evaluated using 25% of the data for testing, 15% for validation,

and the remaining 60% for training purposes. Figure 4 illustrates the results obtained from 80 test samples, showcasing a comparison between Ansys FEA simulations and the leading predictive models, including the proposed approach. Stepwise linear regression and ensemble learning methods were chosen for this comparison due to their favorable MSE values, as summarized in Table 1. As shown, the ResML-HybNN model demonstrates strong agreement with the Ansys Maxwell outputs in estimating both the coupling coefficient and mutual inductance. Specifically, for the coupling coefficient, the ensemble method emerges as the next best performer after the proposed model, followed by the stepwise regression. Conversely, in the case of mutual inductance, the stepwise method shows better alignment than the ensemble, securing the second-best position.

Table 1. Performance comparison with state-of-the-art models in terms of Mean Squared Error (MSE) for Coupling Coefficient, Magnetic Flux, and Mutual Inductance.

Methods	**Kernel**	**MSE**		
		Coupling Coeff.	**Mag. Flux**	**Mutual Ind.**
BiLSTM → LSTM → FC1	-	1.76×10^{-8}	2.01×10^{-6}	4.34×10^{-8}
Gaussian Process Regression	Gaussian	1.71×10^{-8}	1.53×10^{-19}	3.23×10^{-8}
MLP Regression	-	2.55×10^{-8}	2.21×10^{-18}	2.66×10^{-8}
SVM Regression	Linear	1.59×10^{-7}	1.52×10^{-19}	2.34×10^{-8}
GRU → BiLSTM → LSTM	-	7.72×10^{-8}	1.11×10^{-8}	2.09×10^{-8}
GRU	-	6.91×10^{-7}	8.16×10^{-7}	1.86×10^{-8}
GRU → BiLSTM	-	9.68×10^{-6}	3.45×10^{-6}	1.82×10^{-8}
LSTM	-	3.54×10^{-7}	1.48×10^{-7}	1.79×10^{-8}
SVM Regression	Gaussian	1.29×10^{-8}	-	1.77×10^{-8}
Ensemble Regression	-	1.16×10^{-9}	5.67×10^{-20}	1.68×10^{-8}
Linear Regression	Linear	1.68×10^{-9}	5.43×10^{-20}	1.66×10^{-8}
StepWise Regression	Linear	1.10×10^{-9}	5.69×10^{-20}	1.59×10^{-8}
SVM Regression	Quadratic	3.12×10^{-6}	1.52×10^{-19}	1.57×10^{-8}
ResML-HybNN	-	**6.31** $\times 10^{-10}$	5.68×10^{-20}	1.51×10^{-8}

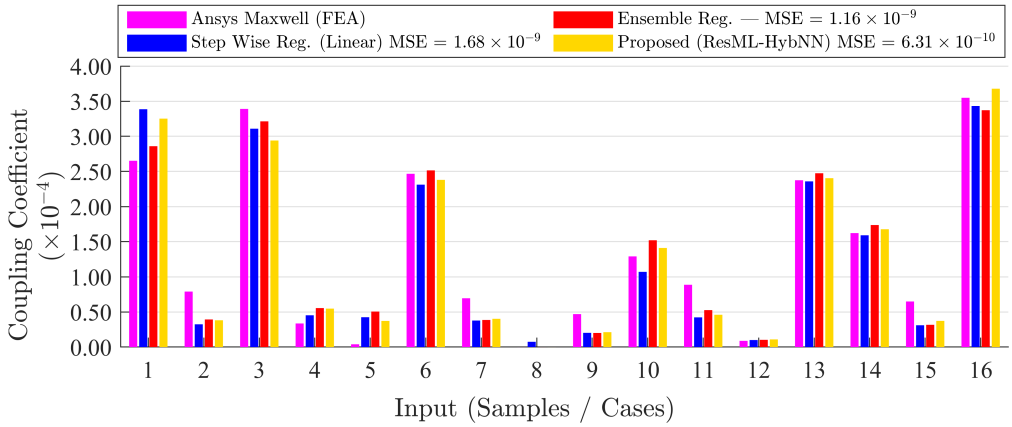


Figure 4. The comparison of the coupling coefficient obtained with ANSYS and those estimated by the two best regression models, as well as the result of the proposed method.

As presented in Table 1, all magnetic flux values predicted by the ResML-HybNN model fall within the FDA's permissible range. Consequently, the sample with the highest estimated coupling was chosen for fabrication. This optimal design features a wire thickness of 0.45 mm, a starting radius of 2.8 mm, a radius increment of 0.1 mm, and a total of 40 turns, as detailed in Table 2. The corresponding ANSYS simulation yielded a mutual inductance of 11.98 µH—the highest value among the evaluated designs, thus making it the preferred coil configuration for the mobile WPT application. The ResML-HybNN model selects coil geometries—such as moderate wire thickness to reduce resistance, a small inner radius to concentrate magnetic flux, fine turn spacing to ensure strong coupling, and a higher number of turns to increase flux linkage—aligning with electromagnetic principles; notably, increasing the turn gap or reducing wire thickness lowers MI due to weaker coupling and higher losses, while increasing wire thickness or reducing the inner radius enhances MI, and excessive increases in radius or spacing reduce field overlap, thereby decreasing MI.

Table 2. Performance of the Proposed HRL-SeqNet for Optimum Coil Geometries, Given in Terms of Mutual Inductance ($\mathcal{R}_{MI}$) of the TX and RX Coils.

Wire Thickness (mm)	Start Radius (mm)	Radius Change (mm)	Total Turns	Mutual Inductance µH
0.45	2.8	0.1	40	12.52

5. Experimental Verification

The experimental setup of the proposed TX, RX coil and the WPT setup is given in Figure 5. Figure 6 shows the fabrication of the Tx and Rx windings, designed based on machine learning estimations. The Tx winding is configured for operation at 140 kHz using a 48nF series resonant capacitor. On the Rx side, the winding is mounted onto 0.5 mm thick solid ferrite cores and paired with series resonant capacitors of 26 nF. Both the Tx and Rx structures consist of planar spiral windings, each starting with an inner radius of 2.8 mm and comprising 40 turns. These windings are constructed using 0.45 mm-thick insulated round copper wire. Table 2 lists the measured mutual inductance values. Slight discrepancies between the simulated and measured results are attributed to fabrication imperfections. The mutual inductance is determined using Equation (1). The mutual inductance M between the transmitter and receiver windings is calculated using the following equation:

$$M = \frac{V_{\text{rms}}}{\omega I_{\text{rms}}} \tag{1}$$

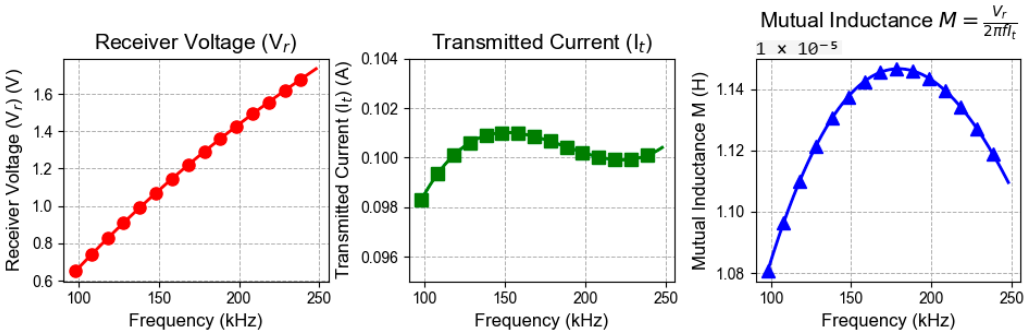


Figure 5. Mutual Inductance analysis for 200 ohm load at various frequencies.

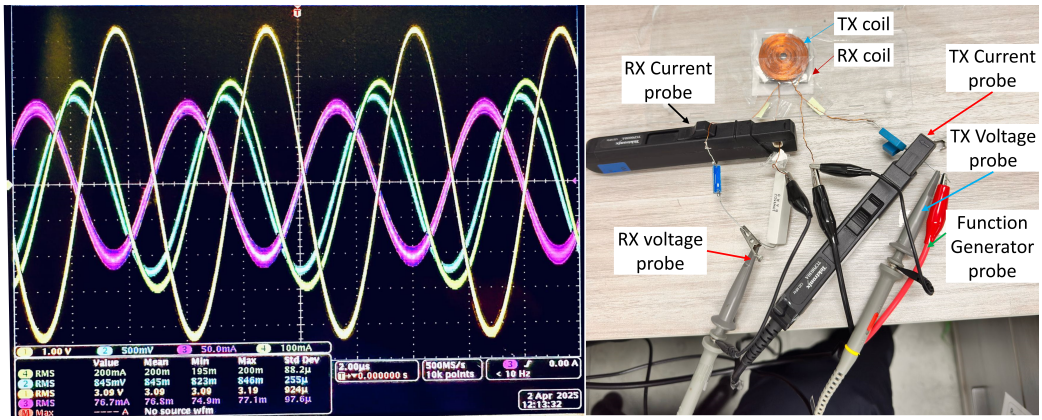
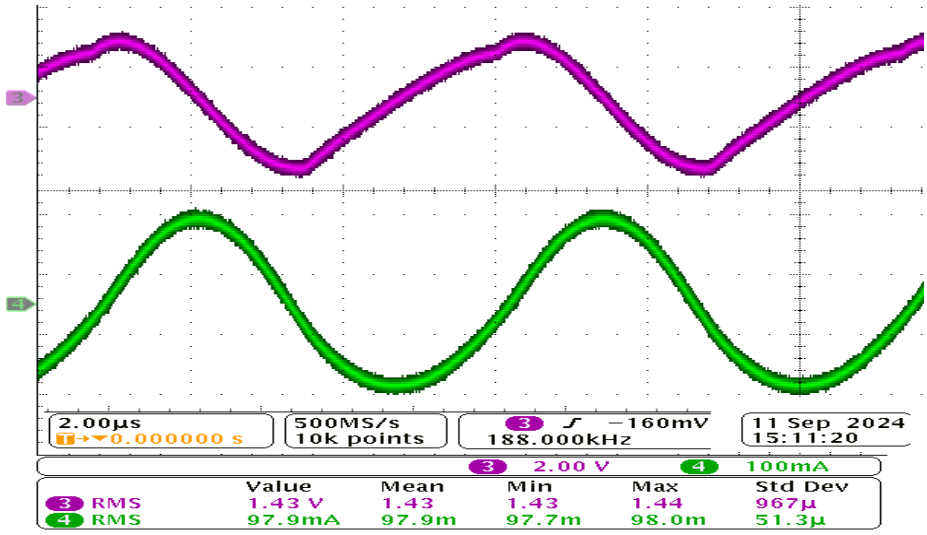


Figure 6. The comparison of the coupling coefficient obtained with ANSYS and those estimated by the two best regression models, as well as the result of the proposed method.

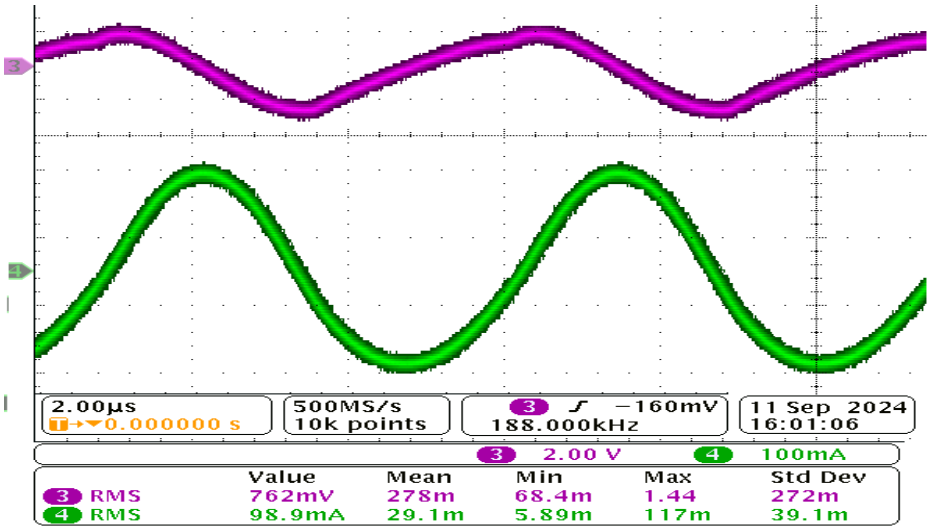
The received voltage in RMS is $V_{\text{rms}} = 845\,\text{mV}$, while the transmitter current is $I_{\text{rms}} = 76.7\,\text{mA}$. The angular frequency, given by $\omega = 2\pi f$, corresponds to the excitation frequency $f = 140\,\text{kHz}$. Using these values, the calculated mutual inductance is $M \approx 12.52\,\mu\text{H}$.

Figure 7 presents the mutual inductance analysis at a resonance frequency of 188 kHz for three different transmitter (Tx) and receiver (Rx) distances: 6 mm, 11 mm, and 16 mm. For each distance, the corresponding values of transmitter voltage (Vt), receiver voltage (Vr), transmitter current (It), receiver current (Ir), mutual inductance (M), and load resistance (R_L) are shown. At 6 mm, the mutual inductance is 12.366 µH with a receiver current of 1.43 A; at 11 mm, it is 6.552 µH with 0.767 A; and at 16 mm, it is 3.888 µH with 0.457 A. The load resistance remains constant at 200 Ohm across all measurements. This analysis demonstrates the decrease in mutual inductance as the distance between Tx and Rx increases.

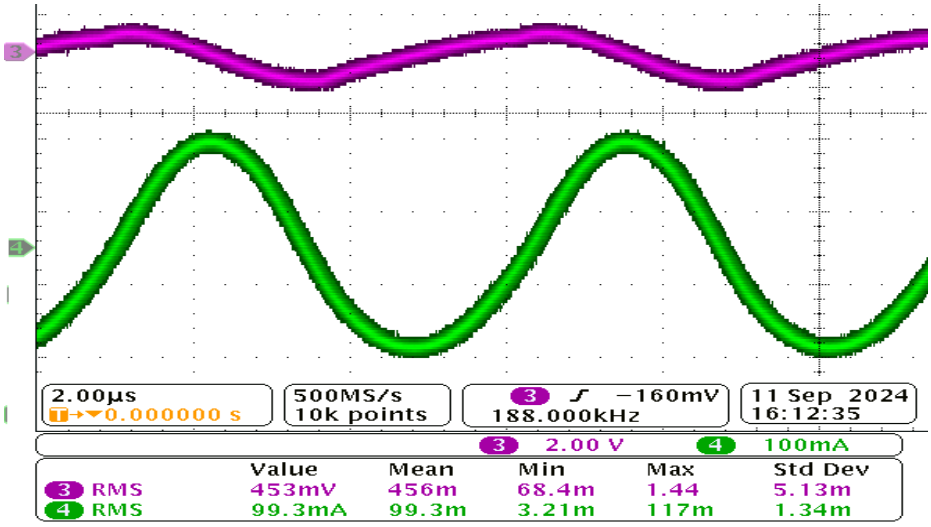


(a) Tx and RX distance of 6mm.

Figure 7. *Cont.*



(b) Tx and RX distance of 11mm.



(c) Tx and RX distance of 16mm.

Figure 7. Mutual Inductance analysis for various distances keeping resonance tuned at 188 kHz.

6. Conclusions

This study presented a machine learning-based framework for optimizing wireless power transfer (WPT) systems targetting mobile device applications. Traditional design approaches often fail to effectively address the nonlinear characteristics of magnetic fields, limiting their capability in optimizing inductive power transfer (IPT) components. The proposed framework, integrating hybrid sequential models, enabled significant improvements in both coil winding and ferrite core design. The optimized configuration, which incorporates a conventional solid ferrite core, achieved a mutual inductance of 12.52 µH, validating the approach's effectiveness. In general, the results demonstrate that the proposed method offers a robust and efficient solution for WPT optimization, improving both system performance and material utilization. This work establishes a foundation for future advancements in electroceutical WPT systems and opens new directions for intelligent design methodologies.

Funding: This Project was funded by KAU Endowment (WAQF) at King Abdulaziz University, Jeddah, under grant no. (WAQF: 238-830-2024). The authors, therefore, acknowledge with thanks WAQF and the Deanship of Scientific Research (DSR) for technical and financial support.

Data Availability Statement: The dataset generated for ML training is publicly available on GitHub at the following URL: https://github.com/fawadmsee20/CoilDesign (accessed on 27 May 2025).

Conflicts of Interest: The author declares no conflict of interest.

References

1. Budhia, M.; Covic, G.A.; Boys, J.T. Design and optimization of circular magnetic structures for lumped inductive power transfer systems. *IEEE Trans. Power Electron.* **2011**, *26*, 3096–3108. [CrossRef]
2. Shen, H.; Tan, P.; Song, B.; Gao, X.; Zhang, B. Receiver position estimation method for multitransmitter WPT system based on machine learning. *IEEE Trans. Ind. Appl.* **2021**, *58*, 1231–1241. [CrossRef]
3. Zhang, W.; Mi, C.C. Compensation topologies of high-power wireless power transfer systems. *IEEE Trans. Veh. Technol.* **2015**, *65*, 4768–4778. [CrossRef]
4. Pahlavan, S.; Shooshtari, M.; Jafarabadi Ashtiani, S. Star-shaped coils in the transmitter array for receiver rotation tolerance in free-moving wireless power transfer applications. *Energies* **2022**, *15*, 8643. [CrossRef]
5. Zhang, X.; Kan, T.; You, C.; Mi, C. Modeling and analysis of AC output power factor for wireless chargers in electric vehicles. *IEEE Trans. Power Electron.* **2016**, *32*, 1481–1492. [CrossRef]
6. Adepoju, W.O.; Bhattacharya, I.; Bima, M.E.; Banik, T. Novel metamaterial and ai-based multi-objective optimization of coil parameters for efficient wireless power transfer. In Proceedings of the 2021 IEEE Vehicle Power and Propulsion Conference (VPPC), Gijon, Spain, 25–28 October 2021; pp. 1–6.
7. Dinis, H.; Mendes, P. A comprehensive review of powering methods used in state-of-the-art miniaturized implantable electronic devices. *Biosens. Bioelectron.* **2021**, *172*, 112781. [CrossRef] [PubMed]
8. Karimi, M.J.; Schmid, A.; Dehollain, C. Wireless power and data transmission for implanted devices via inductive links: A systematic review. *IEEE Sens. J.* **2021**, *21*, 7145–7161. [CrossRef]
9. Benjamens, S.; Dhunnoo, P.; Meskó, B. The state of artificial intelligence-based FDA-approved medical devices and algorithms: An online database. *NPJ Digit. Med.* **2020**, *3*, 118. [CrossRef]
10. Ma, J.; Jiang, X.; Fan, A.; Jiang, J.; Yan, J. Image matching from handcrafted to deep features: A survey. *Int. J. Comput. Vis.* **2021**, *129*, 23–79. [CrossRef]
11. Fawad; Khan, M.J.; Riaz, M.A.; Shahid, H.; Khan, M.S.; Amin, Y.; Loo, J.; Tenhunen, H. Texture representation through overlapped multi-oriented tri-scale local binary pattern. *IEEE Access* **2019**, *7*, 66668–66679.
12. Shakoor, M.H.; Boostani, R. A novel advanced local binary pattern for image-based coral reef classification. *Multimed. Tools Appl.* **2018**, *77*, 2561–2591. [CrossRef]
13. Shihavuddin, A.; Gracias, N.; Garcia, R.; Gleason, A.C.; Gintert, B. Image-based coral reef classification and thematic mapping. *Remote Sens.* **2013**, *5*, 1809–1841. [CrossRef]
14. Shrestha, A.; Mahmood, A. Review of deep learning algorithms and architectures. *IEEE Access* **2019**, *7*, 53040–53065. [CrossRef]
15. Sarkar, D.; Khan, T.; Talukdar, F.A.; Rengarajan, S.R. Computational Intelligence for Modeling and Optimization of RFEH and WPT Systems: A Comprehensive Survey: Computational Intelligence for RFEH and WPT Systems. *IEEE Microw. Mag.* **2023**, *24*, 46–60. [CrossRef]
16. Ali, A.; Mohd Yasin, M.N.; Jusoh, M.; Ahmad Hambali, N.A.M.; Abdul Rahim, S.R. Optimization of wireless power transfer using artificial neural network: A review. *Microw. Opt. Technol. Lett.* **2020**, *62*, 651–659. [CrossRef]
17. Shimokawa, S.; Oshima, H.; Shimizu, K.; Uehara, Y.; Fujisaki, J.; Furuya, A.; Igarashi, H. Fast 3-D optimization of magnetic cores for loss and volume reduction. *IEEE Trans. Magn.* **2018**, *54*, 1–4. [CrossRef]
18. Pretorius, K.; Pillay, N. Neural network crossover in genetic algorithms using genetic programming. *Genet. Program. Evolvable Mach.* **2024**, *25*, 1–30. [CrossRef]
19. Jeong, M.S.; Jang, J.H.; Lee, E.S. Optimal IPT core design for wireless electric vehicles by Reinforcement Learning. *IEEE Trans. Power Electron.* **2023**, *38*, 13262–13272. [CrossRef]
20. Dixit, P.; Silakari, S. Deep learning algorithms for cybersecurity applications: A technological and status review. *Comput. Sci. Rev.* **2021**, *39*, 100317. [CrossRef]
21. Vinayakumar, R.; Alazab, M.; Soman, K.; Poornachandran, P.; Al-Nemrat, A.; Venkatraman, S. Deep learning approach for intelligent intrusion detection system. *IEEE Access* **2019**, *7*, 41525–41550. [CrossRef]
22. Liu, G.; Bao, H.; Han, B. A stacked autoencoder-based deep neural network for achieving gearbox fault diagnosis. *Math. Probl. Eng.* **2018**, *2018*, 1–10. [CrossRef]

23. Alrawashdeh, K.; Purdy, C. Fast hardware assisted online learning using unsupervised deep learning structure for anomaly detection. In Proceedings of the 2018 International Conference on Information and Computer Technologies (ICICT), DeKalb, IL, USA, 23–25 March 2018; pp. 128–134.
24. Young, T.; Hazarika, D.; Poria, S.; Cambria, E. Recent trends in deep learning based natural language processing. *IEEE Comput. IntelligenCe Mag.* **2018**, *13*, 55–75. [CrossRef]
25. Nguyen, T.T.; Reddi, V.J. Deep reinforcement learning for cyber security. *IEEE Trans. Neural Netw. Learn. Syst.* **2021**, *34*, 3779–3795. [CrossRef] [PubMed]
26. Lin, Z.; Shi, Y.; Xue, Z. Idsgan: Generative adversarial networks for attack generation against intrusion detection. In *Pacific-Asia Conference on Knowledge Discovery and Data Mining*; Springer: Berlin/Heidelberg, Germany, 2022; pp. 79–91.

Disclaimer/Publisher's Note: The statements, opinions and data contained in all publications are solely those of the individual author(s) and contributor(s) and not of MDPI and/or the editor(s). MDPI and/or the editor(s) disclaim responsibility for any injury to people or property resulting from any ideas, methods, instructions or products referred to in the content.